

# UCSF

## UC San Francisco Previously Published Works

### Title

$\Delta$ Np63 $\alpha$ -induced DUSP4/GSK3 $\beta$ /SNAI1 pathway in epithelial cells drives endometrial fibrosis

### Permalink

<https://escholarship.org/uc/item/22h911kq>

### Journal

Cell Death & Disease, 11(6)

### ISSN

2041-4889

### Authors

Zhao, Guangfeng  
Li, Ruotian  
Cao, Yun  
[et al.](#)

### Publication Date

2020

### DOI

10.1038/s41419-020-2666-y

Peer reviewed

ARTICLE

Open Access

# $\Delta$ Np63 $\alpha$ -induced DUSP4/GSK3 $\beta$ /SNAI1 pathway in epithelial cells drives endometrial fibrosis

Guangfeng Zhao<sup>1</sup>, Ruotian Li<sup>2</sup>, Yun Cao<sup>1</sup>, Minmin Song<sup>1</sup>, Peipei Jiang<sup>1</sup>, Qianwen Wu<sup>3</sup>, Zhenhua Zhou<sup>4</sup>, Hui Zhu<sup>1</sup>, Huiyan Wang<sup>1</sup>, Chenyan Dai<sup>1</sup>, Dan Liu<sup>1</sup>, Simin Yao<sup>1</sup>, Haining Lv<sup>3</sup>, Limin Wang<sup>3</sup>, Jianwu Dai<sup>5</sup>, Yan Zhou<sup>6</sup> and Yali Hu<sup>1</sup>

## Abstract

Epithelial homeostasis plays an essential role in maintaining endometrial function. But the epithelial role in endometrial fibrosis has been less studied. Previously, we showed that ectopic expression of  $\Delta$ Np63 $\alpha$  is associated with fibrosis process and epithelial dysfunction in endometria of patients with intrauterine adhesions (IUA). Since  $\Delta$ Np63 $\alpha$  is profoundly involved in maintaining the epithelial homeostasis, we hereby focused on its roles in regulating the function and phenotype of endometrial epithelial cells (EECs) in context of endometrial fibrosis. We identified a typical type 2 epithelial-to-mesenchymal transition (EMT) in EECs from IUA patients and this process was induced by the forced expression of  $\Delta$ Np63 $\alpha$  in EECs. In transcriptomic analysis, we found that diverse signaling pathways regulated by  $\Delta$ Np63 $\alpha$  were involved in pro-EMT. We demonstrated that the DUSP4/GSK-3 $\beta$ /SNAI1 pathway was critical in transducing the pro-EMT signals initiated by  $\Delta$ Np63 $\alpha$ , while bFGF reversed  $\Delta$ Np63 $\alpha$ -induced EMT and endometrial fibrosis both in vitro and in vivo by blocking DUSP4/GSK3 $\beta$ /SNAI1 pathway. Taken together, our findings are important to understand the molecular mechanisms of endometrial fibrosis and to provide potential therapeutic targets.

## Introduction

Epithelial homeostasis is essential for tissue function<sup>1,2</sup>. Loss of the epithelial homeostasis leads to tissue remodeling and dysfunction<sup>3</sup>. In spite of cyclical endometrial shedding and rehealing in every menstrual cycle, the epithelial homeostasis in endometrium is well-developed and maintained. The mechanism to maintain the relatively stable epithelial phenotype in endometrial epithelial cells (EECs) remains largely unknown<sup>4</sup>. Since epithelium is directly exposed to exogenous injuries, such as intrauterine procedures, it is likely that these injuries disrupt the epithelial homeostasis and result in local tissue

remodeling and dysfunction<sup>5</sup>. Endometrial fibrosis is the commonest pathology following intrauterine procedures and its mechanisms remain elusive<sup>6</sup>. Especially, the contributions of epithelial dysfunction and the molecular processes involved in the epithelial dysfunction have not well been characterized. The usual phenotype of disrupted epithelial homeostasis is epithelial–mesenchymal-transition (EMT), in which the epithelial cells have the changed phenotype and lose the polarity, while the cells gain the mesenchymal phenotype and motility<sup>7</sup>. Given that EMT is closely involved in the fibrosis of other organs such as kidneys and lungs, we hypothesized that EMT might be involved in the development of endometrial fibrosis.

Previously, we revealed that a  $\Delta$ Np63 $\alpha$  + lineage emerges in the endometria of patients with IUAs<sup>8</sup>.  $\Delta$ Np63 $\alpha$  is the main form of p63 in epithelial cells<sup>9</sup>. It is known that during uterine development, p63 is expressed in the epithelial cells of the paramesonephric ducts but is no longer expressed in EECs after the fusion of bilateral paramesonephric ducts<sup>10</sup>. The expansion of the p63 lineage in pathological conditions is associated with

Correspondence: Jianwu Dai (jwdai@genetics.ac.cn) or Yan Zhou (yan.zhou@ucsf.edu) or Yali Hu (yalihu@nju.edu.cn)

<sup>1</sup>Department of Obstetrics and Gynecology, The Affiliated Drum Tower Hospital of Nanjing University Medical School, 321 Zhongshan Rd., Nanjing 210008, China

<sup>2</sup>Department of Laboratory Medicine, Jiangsu Key Laboratory for Molecular Medicine, Nanjing University Medical School, 321 Zhongshan Rd., Nanjing 210008, China

Full list of author information is available at the end of the article  
These authors contributed equally: Guangfeng Zhao, Ruotian Li, Yun Cao  
Edited by E. Candi

© The Author(s) 2020



**Open Access** This article is licensed under a Creative Commons Attribution 4.0 International License, which permits use, sharing, adaptation, distribution and reproduction in any medium or format, as long as you give appropriate credit to the original author(s) and the source, provide a link to the Creative Commons license, and indicate if changes were made. The images or other third party material in this article are included in the article's Creative Commons license, unless indicated otherwise in a credit line to the material. If material is not included in the article's Creative Commons license and your intended use is not permitted by statutory regulation or exceeds the permitted use, you will need to obtain permission directly from the copyright holder. To view a copy of this license, visit <http://creativecommons.org/licenses/by/4.0/>.

pulmonary fibrotic lesions<sup>11,12</sup>, suggesting that p63 functions in maintaining the homeostasis of epithelial tissues and is likely associated with fibrotic lesions. However, it is unclear how the ectopic expression of p63 in endometrium affects the epithelial homeostasis. As we found that the administration of autologous bone marrow stem cells to the uterine cavity in IUA patients reduced the  $\Delta$ Np63 $\alpha$  + lineage, restored the endometria response to sex hormones, alleviated endometrial fibrosis, attained successful pregnancy, and finally delivered term babies<sup>8</sup>, we hypothesized that  $\Delta$ Np63 $\alpha$  may promote endometrial fibrosis by driving EMT, and if it does, the therapy with antagonizing  $\Delta$ Np63 $\alpha$  could restore functional endometria by reversing EMT.

To test our hypotheses, we conducted various experiments in vitro and in vivo, and in IUA patients. We demarcated the roles of type 2 EMT in fibrotic endometria, and identified a novel signal pathway DUSP4/GSK3 $\beta$ /Snail. Moreover, we demonstrated that tissue regeneration factor, basic fibroblast growth factor (bFGF), could antagonize the effects of  $\Delta$ Np63 $\alpha$  and reverse EMT and endometrial fibrosis. The present study advances our understanding of cellular and molecular mechanisms of endometrial fibrosis and provides insights into novel therapeutic targets.

## Materials and methods

### Patients and clinical information

Patients with IUA who underwent hysteroscopy adhesiolysis at the Affiliated Drum Tower Hospital of Nanjing University from January 2014 to December 2016. Written informed consent was obtained from each participant. This study was approved by the Committee on Human Research of the Nanjing Drum Tower Hospital (No. 2012022). The diagnosis of IUA was based on criteria recommended by the American Fertility Society<sup>13</sup>. Totally, 69 patients with severe IUA were initially included. Of them, 16 had only detectable mRNA of  $\Delta$ Np63 $\alpha$  by quantitative polymerase chain reaction (qPCR), 2 were positive  $\Delta$ Np63 $\alpha$  protein only in IHC, 30 were positive both in qPCR and IHC, and remaining 21 had undetectable mRNA and protein in qPCR and IHC. Those 30 patients with detectable mRNA and protein were selected in the further experiments. The patients had normal ovary function. The control group was comprised of 30 patients with a normal endometrium and ovaries, as assessed by hysteroscopy and ultrasonography during infertility screening. The clinical information of all participants is summarized in Supplemental Table 1.

### RNA-seq read processing, assembly, and transcriptome sequence analysis

For the RNA-seq of EECs, total RNA was prepared using an RNeasy Plus Micro Kit (Qiagen, Dusseldorf,

Germany). The RNA purity was assessed using a Nano Drop spectrophotometer, the RNA concentration was assessed using a Qubit 3.0 fluorometer and the RNA integrity was assessed using an Agilent 2100 Bioanalyzer. The sequencing library was prepared following the instruction manual of a VAHTS total RNA-seq (H/M/R) Library Prep Kit for Illumina<sup>®</sup> (Vazyme, China). To isolate the appropriate cDNA fragment size for sequencing, the library fragments were selected with VAHTSTM DNA Clean Beads. The enzyme UDG was used to digest the second strand of cDNA. PCR amplification was performed, and the products were purified. After cluster generation, the libraries were sequenced on an Illumina HiSeq X10 platform (Illumina, California, USA), and 150-bp paired-end reads were generated. Raw reads in the FASTQ format were first processed using in-house Perl scripts. Then, the processed reads were mapped to the reference genome. The reference genome and gene model annotation files were downloaded directly from the genome website. The reference genome index was built using hisat2-build<sup>14</sup>, and paired-end clean reads were aligned to the reference genome using Hisat2 (v2.0.5)<sup>15</sup>.

### mRNA differential expression analysis

Cuffdiff (v1.3.0)<sup>16</sup> was used to calculate the fragments per kilobase of exon per million reads mapped (FPKMs) for coding genes in each sample. Gene FPKMs were computed by summing the FPKMs of the transcripts in each gene group, and FPKMs were calculated based on the length of the fragments and the read counts mapped to each fragment. Cuffdiff (v2.2.1)<sup>16</sup> provides statistical methods for determining differential expression in digital transcript or gene expression datasets using a model based on a negative binomial distribution. Transcripts or genes with corrected *p* values less than 0.05 and an absolute value of log<sub>2</sub> (fold change) >1 were defined as being significantly differentially expressed gene (DEG). Heatmaps were generated using pheatmap in R principal component analysis. Gene ontology (GO) enrichment analysis of DEGs was performed with a Perl module (GO::TermFinder). GO terms with corrected *p* values less than 0.05 were significantly enriched among the DEGs.

### IUA-like mouse model

Animal experiments were approved by the Institutional Animal Care and Use Committee at the Nanjing Drum Tower Hospital, Nanjing University Medical School. Eight-week-old BALB/c female virgin mice, weighing 18–20 g, were purchased from the Experimental Animal Center of Nanjing Medical University (Nanjing, China). Mouse model of endometrial fibrosis was established by dual (mechanical and inflammation) methods using uterine curettage and lipopolysaccharide (LPS) injection as previously described<sup>17</sup>. Briefly, the mouse model was

created at estrum, which corresponds to the late reproductive phase in humans, based on vaginal smears<sup>18,19</sup>. All the mice were anesthetized with 4% chloral hydrate (10 mg/kg) through intraperitoneal injections. The uterus was exposed and the horn was damaged with a rough surface needle that was inserted all the way through the lumen and scratched up and down for 2 min until the uterine wall became rough. A single dose of 20  $\mu$ l LPS (10 mg/ml, derived from *Escherichia coli* 0111: B4; Sigma, St. Louis, MO, USA) was administered via intrauterine injection to cause endometrial injury, and the ends were clamped with tweezers for 5 min. A vertical incision was made in the abdominal wall of control mice. Mouse models were randomly assigned at a 1:1:1 ration into three groups: (a) the sham group, (b) the PBS group, and (c) the bFGF treatment group. The treatment groups received 2 intrauterine injections with 20  $\mu$ l PBS or bFGF (100 mg/kg) 7 days apart, and the ends were clamped with tweezers for 5 min. After the surgery, mice were intramuscularly injected (thigh) with penicillin (20,000 U/day) for 3 days. Mice were sacrificed at the fifth estrous periods (approximately 28 days) after injury and all the uteruses were collected at estrum.

Some specimens from each group were fixed in formaldehyde and embedded in paraffin. Five-micron sections were cut and stained with hematoxylin and eosin (H&E) as well as Masson stain to evaluate the histological evidence of fibrosis in a blinded manner. Other specimens were used for quantitative real time PCR and western blotting. The antibodies used in this study are listed in Supplemental Table 2.

### Statistics

Statistical analyses were performed using GraphPad Prism software (version 5.01, San Diego, CA). The data are presented as the mean  $\pm$  standard deviation for the number of independent experiments indicated in each figure legend. One-way ANOVA followed by a Student–Newman–Keuls multiple comparisons test were used to compare three or more experimental groups. A Student's *t* test was used for comparisons of two experimental groups when the data were normally distributed. When the data were not normally distributed, a non-parametric test was used. Statistical significance was defined as  $p < 0.05$ .

More details of Materials and methods are provided in Supplementary materials.

## Results

### $\Delta$ Np63 $\alpha$ lineage expansion is associated with EEC–EMT in the endometrium of patients with IUA

Endometrial fibrosis in IUA patients is characterized with scarring under hysteroscopic observation, however, it is not clear whether luminal epithelium slough from the

mesenchymal layer or whether these cells lose their epithelial properties. To clarify this issue, we performed the various experiments in the endometrial sections from 30 patients who showed significant elevation of mRNA and protein of  $\Delta$ Np63 $\alpha$  in endometrial biopsy.

We compared the distribution of the  $\Delta$ Np63 $\alpha$ -positive lineage in the luminal and glandular epithelia of endometria by immunohistochemistry.  $\Delta$ Np63 $\alpha$  + lineage presented focal distribution. As depicted in Fig. 1a, b and Supplementary Fig. 1A, the  $\Delta$ Np63 $\alpha$  + lineage could expand along the luminal epithelium of the endometrium, or in the glandular epithelium. Overall, 40  $\Delta$ Np63 $\alpha$  positive foci were identified on the endometrial sections prepared from the 30 IUA patients. Of 40  $\Delta$ Np63 $\alpha$  positive foci, 25 were located in the luminal epithelial regions, 4 were located in the glandular epithelial regions, and 11 were located in both the luminal and glandular epithelial regions. To further confirm whether  $\Delta$ Np63 $\alpha$  is expressed in epithelial cells, immunofluorescence co-localization of  $\Delta$ Np63 $\alpha$  and CK was performed and the results showed that  $\Delta$ Np63 $\alpha$  and CK were located in the same cells by confocal laser microscopy (Supplementary Fig. 2).

Masson's trichrome staining showed that collagen staining was detected not only in endometrial stroma, but also in luminal EECs in IUAs, suggesting that EECs lost their epithelial properties and gained mesenchymal features (Fig. 1c, d, Supplementary Fig. 1B).

To examine whether the endometrial epithelium undergoes EMT in IUAs, we analyzed the expression of CK, E-cadherin, N-cadherin,  $\alpha$ -smooth muscle actin ( $\alpha$ -SMA), and vimentin in endometrial biopsies. As shown in Fig. 1e–l, while EECs remained to express CK (Supplementary Fig. 1C), E-cadherin was globally downregulated on luminal and glandular EECs (Fig. 1e, f), but N-cadherin was intensively upregulated on both epithelial and stromal cells (Fig. 1g, h). Vimentin, a hallmark of stromal cells, was also upregulated in epithelial cells (Fig. 1i, j). Notably,  $\alpha$ -SMA was upregulated in both luminal and glandular epithelial cells (Fig. 1k, l). To verify the co-localization of  $\Delta$ Np63 $\alpha$  and CK, E-cadherin, N-cadherin, and  $\alpha$ -SMA, we performed immunofluorescence staining and found that they were co-located in EEC with confocal microscopy (Fig. 1m). These phenotype changes were consistent with type 2 EMT.

### $\Delta$ Np63 $\alpha$ enriches the transcription of genes that promote EMT in EECs

As we found the  $\Delta$ Np63 $\alpha$  expression in EECs from the IUA patients (Fig. 1), we further examined whether  $\Delta$ Np63 $\alpha$  + lineage expansion induces EEC–EMT. Primary EECs (>95% purity identified with CK stain as shown in Supplementary Fig. 3) from normal controls were infected with either Ad- $\Delta$ Np63 $\alpha$  or Ad-CTL. After 24 h, the RNA was extracted and subjected to RNA sequencing (RNA-

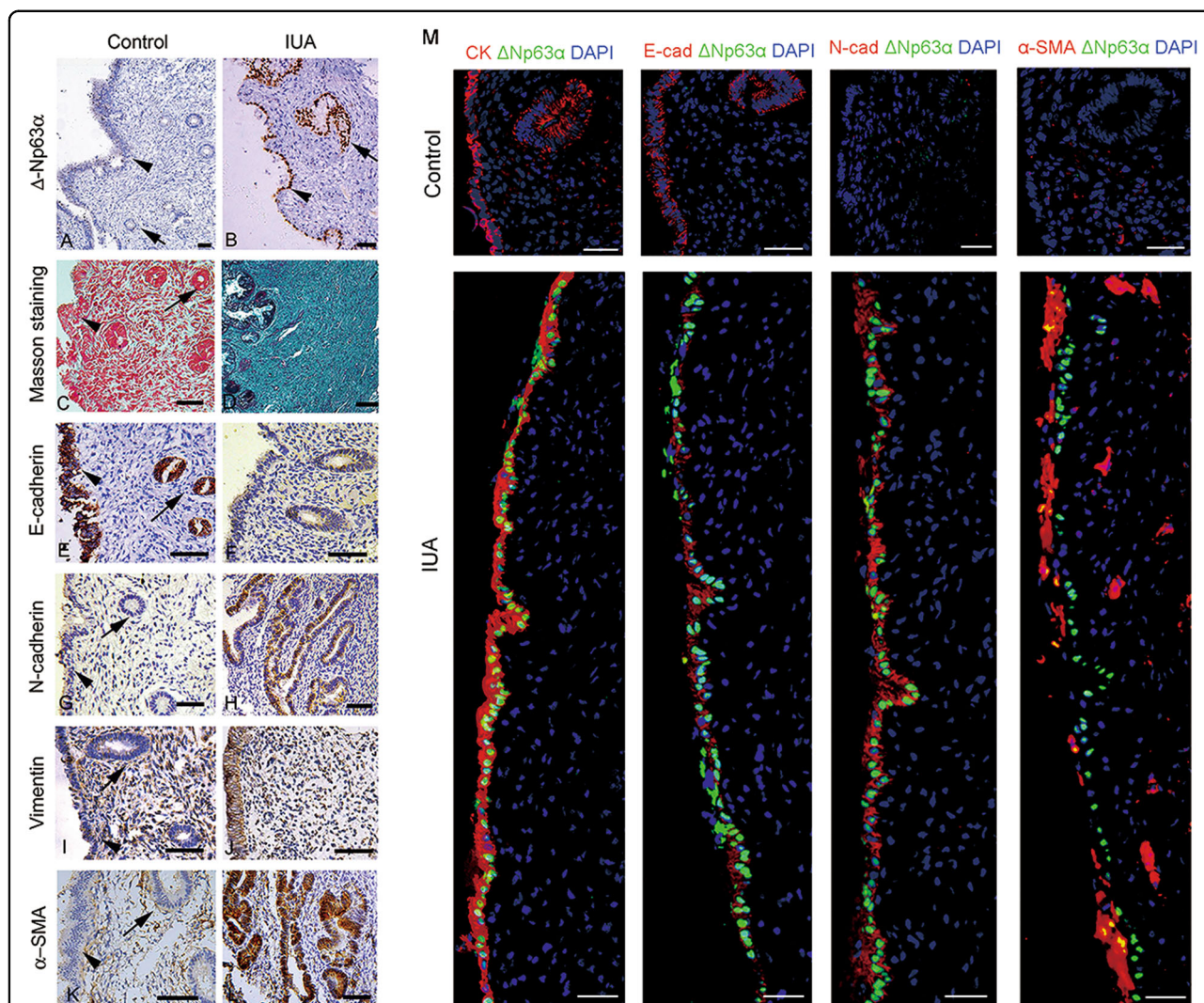


**Fig. 1** EEC–EMT is associated with ΔNp63α upregulation in endometrial biopsies from IUA patients. **a, b** Representative images of ΔNp63α immunostaining in endometrial biopsies of normal ( $n = 30$ ) and fibrotic endometria ( $n = 30$ ). **c, d** Representative images of Masson staining in normal ( $n = 30$ ) and fibrotic endometria ( $n = 30$ ). **e, f** Representative images of E-cadherin immunostaining in endometrial biopsies of normal ( $n = 30$ ) and fibrotic endometria ( $n = 30$ ). **g, h** Representative images of N-cadherin immunostaining in endometrial biopsies of normal ( $n = 30$ ) and fibrotic endometria ( $n = 30$ ). **i, j** Representative images of Vimentin immunostaining in endometrial biopsies of normal ( $n = 30$ ) and fibrotic endometria ( $n = 30$ ). **k, l** Representative images of α-SMA immunostaining in endometrial biopsies of normal ( $n = 30$ ) and fibrotic endometria ( $n = 30$ ). Scale bars, 50 μm. Arrowhead: luminal epithelial cells; arrow: glandular epithelial cells. **m** Representative images of colocation of ΔNp63α with cytokeratin (CK), E-cadherin, N-cadherin, or α-SMA in endometrial biopsies of normal ( $n = 5$ ) and fibrotic endometria ( $n = 5$ ). Scale bars, 25 μm.

seq) analysis. As shown in the volcano plot (Fig. 2a), 348 genes were differentially expressed in Ad-ΔNp63α- and Ad-CTL-infected EECs. The hierarchical clustering analysis of DEGs separated into two groups (Fig. 2b). ΔNp63α overexpression induced the upregulation of 146 genes and the downregulation of 202 genes in EECs (Supplementary Table 3). To verify the DEGs, we conducted qPCR to examine the mRNA levels of ten mostly upregulated and downregulated genes, and the results showed same differential expression patterns as those in RNA-seq (Supplementary Fig. 4).

Gene ontology (GO) enrichment analyses identified 7 biological processes from the upregulated genes and 20 biological processes from the downregulated genes ( $p < 0.05$ , Supplementary Table 4). Terms related to cellular aromatic compound metabolic processes, chromosome segregation, cell death, autophagy, and the regulation of cell activation and growth were significantly associated with the downregulated genes (Fig. 2c). Terms related to the positive regulation of immune effector processes, such as mast cell activation, leukocyte and myeloid leukocyte activation, and the inhibition of autophagy and the

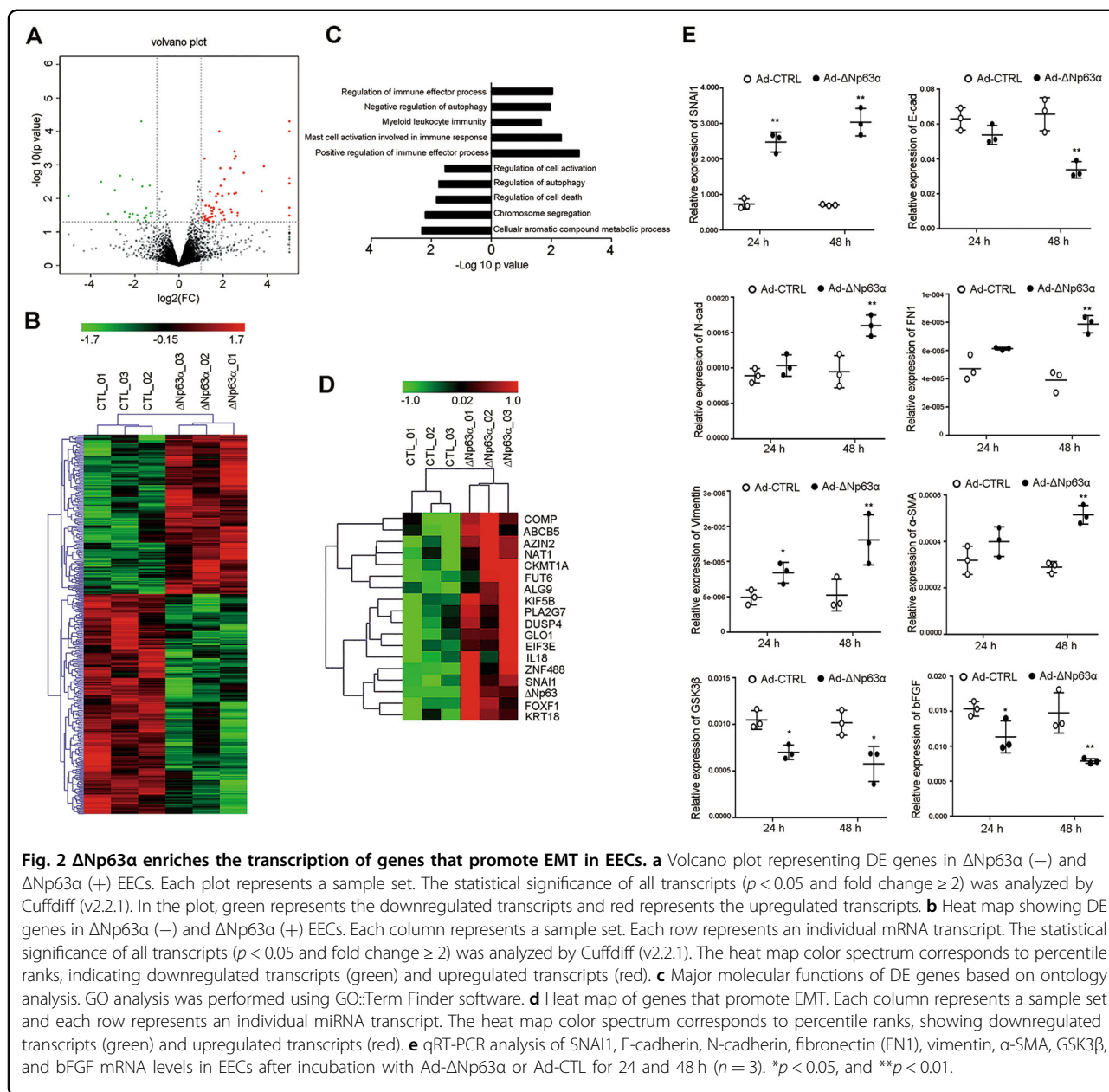
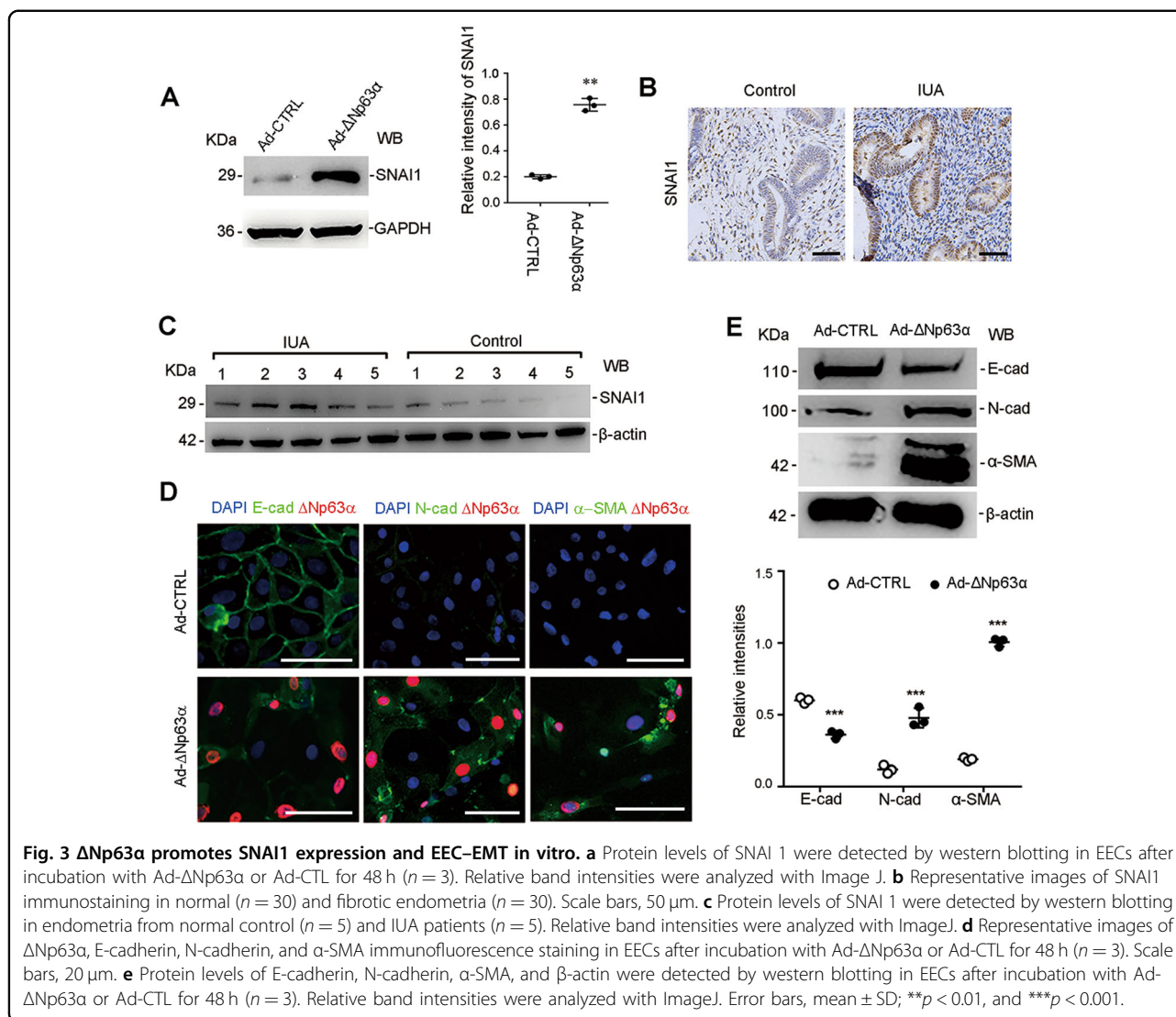


**Fig. 2**  $\Delta\text{Np63}\alpha$  enriches the transcription of genes that promote EMT in EECs. **a** Volcano plot representing DE genes in  $\Delta\text{Np63}\alpha$  (-) and  $\Delta\text{Np63}\alpha$  (+) EECs. Each plot represents a sample set. The statistical significance of all transcripts ( $p < 0.05$  and fold change  $\geq 2$ ) was analyzed by Cuffdiff (v2.2.1). In the plot, green represents the downregulated transcripts and red represents the upregulated transcripts. **b** Heat map showing DE genes in  $\Delta\text{Np63}\alpha$  (-) and  $\Delta\text{Np63}\alpha$  (+) EECs. Each column represents a sample set. Each row represents an individual mRNA transcript. The statistical significance of all transcripts ( $p < 0.05$  and fold change  $\geq 2$ ) was analyzed by Cuffdiff (v2.2.1). The heat map color spectrum corresponds to percentile ranks, indicating downregulated transcripts (green) and upregulated transcripts (red). **c** Major molecular functions of DE genes based on ontology analysis. GO analysis was performed using GO::Term Finder software. **d** Heat map of genes that promote EMT. Each column represents a sample set and each row represents an individual miRNA transcript. The heat map color spectrum corresponds to percentile ranks, showing downregulated transcripts (green) and upregulated transcripts (red). **e** qRT-PCR analysis of SNAI1, E-cadherin, N-cadherin, fibronectin (FN1), vimentin,  $\alpha$ -SMA, GSK3 $\beta$ , and bFGF mRNA levels in EECs after incubation with Ad- $\Delta\text{Np63}\alpha$  or Ad-CTRL for 24 and 48 h ( $n = 3$ ). \* $p < 0.05$ , and \*\* $p < 0.01$ .

formation of the primary germ layer, were associated with the upregulated genes (Fig. 2c). Based on the GO terms from both upregulated and downregulated genes,  $\Delta\text{Np63}\alpha$  appears to promote the immune response and inflammation, to repress chromosome segregation and cell proliferation and development. All these biological processes have been demonstrated to be the driving factors in the induction of pathological EMT<sup>20–23</sup>.

During further screening of genes involved in EMT from  $\Delta\text{Np63}\alpha$ -induced EEC-transcriptomes, 18 genes that promote EMT were identified, including SNAI1, a key EMT driver. Hierarchical clustering analysis separated

these 18 genes into two groups (Fig. 2d). By dissecting the SNAI1-mediated signaling pathway, we showed that SNAI1 was upregulated 24 h after Ad- $\Delta\text{Np63}\alpha$  infection, while the SNAI1-mediated downregulation of CDH1 (E-cadherin) and upregulation of CDH2 (N-cadherin),  $\alpha$ -SMA, VIM (vimentin), and FN (fibronectin) were not detected even 48 h after infection (Fig. 2e). However, GSK3 $\beta$ , a protein kinase that promotes SNAI1-ubiquitination and -degradation was downregulated both at 24 and 48 h. And bFGF expression was also downregulated both at 24 and 48 h (Fig. 2e). Thus, multiple molecules might be involved in SNAI1 activation.



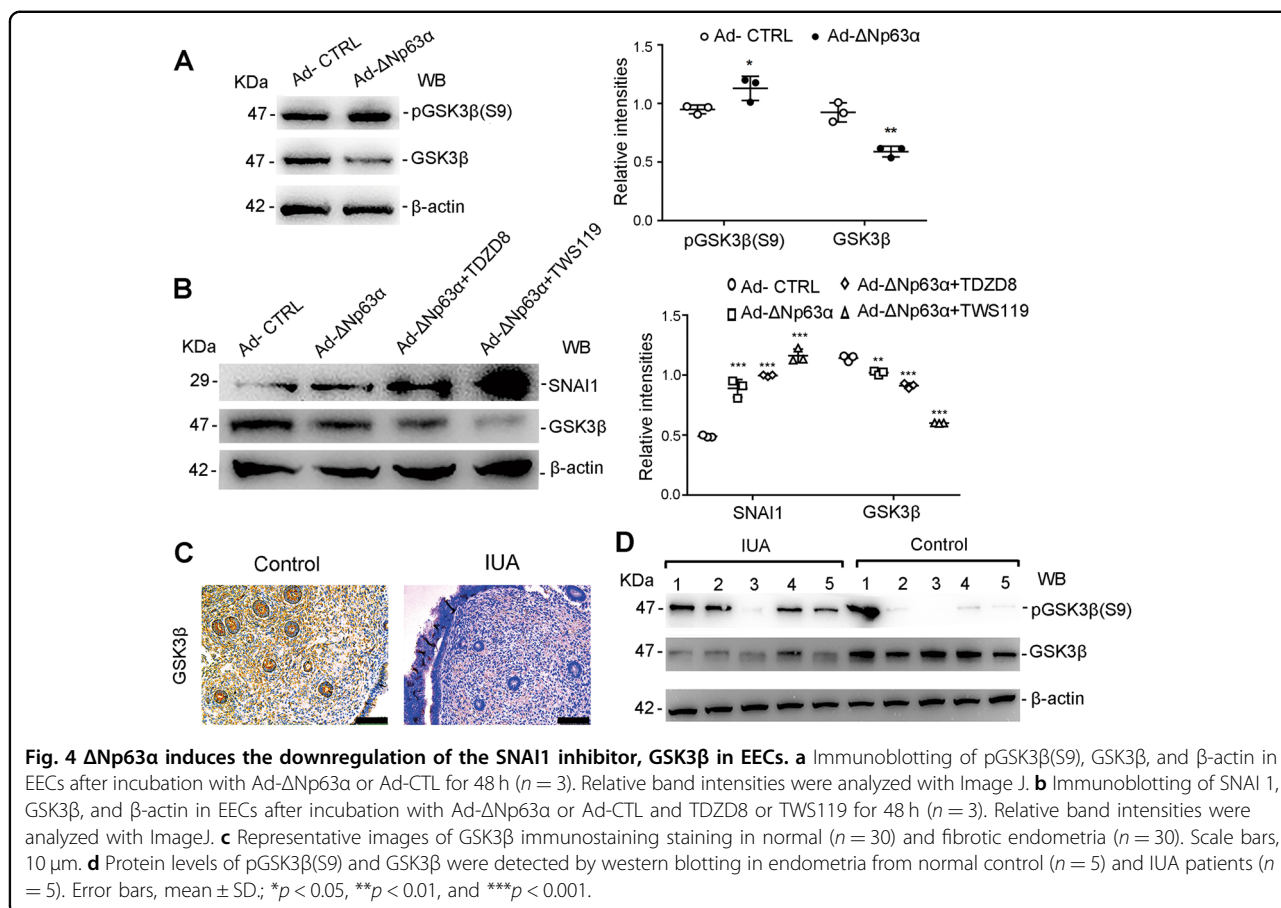
**$\Delta$ Np63 $\alpha$  induces the activation of SNAI1 signaling in EECs in vitro and in the endometria from IUA patients**

The enhanced transcription of genes in EECs transfected with  $\Delta$ Np63 $\alpha$  (Fig. 2e) suggested that  $\Delta$ Np63 $\alpha$  induced a SNAI1-mediated phenotypic shift from an epithelial to a mesenchymal phenotype. Therefore, we examined the  $\Delta$ Np63 $\alpha$ -induced expression of the SNAI1 protein and SNAI1’s downstream proteins.

As shown in Fig. 3a, SNAI1 protein level in primary EECs infected with Ad- $\Delta$ Np63 $\alpha$  had a fourfold increase compared to that in the cells infected with Ad-CTRL. Critically, the SNAI1 protein in the endometria from IUA patients was also significantly upregulated in immunostaining (Fig. 3b) and immunoblotting (Fig. 3c). Meanwhile, E-cadherin, a key target of SNAI1, was downregulated in the immunostaining (Fig. 3d) and Western blotting showed that E-cadherin protein expression decreased to 59% of the control expression

level (Fig. 3e). The  $\Delta$ Np63 $\alpha$ -induced upregulation of the N-cadherin and  $\alpha$ -SMA proteins was further confirmed by immunostaining (Fig. 3d) and Western blotting displayed that N-cadherin and  $\alpha$ -SMA proteins in the cells infected with Ad- $\Delta$ Np63 were increased by 4- and 5.2-fold respectively, compared to those in EECs infected with the control plasmid (Fig. 3e).

To further confirm the role of SNAI1 in  $\Delta$ Np63 $\alpha$ -induced EEC-EMT, we constructed a high expression vector of SNAI1 (pcDNA3.1-SNAI1). Then pcDNA3.1-SNAI1 or empty control vector was transfected into EECs with lipo3000. After 48 h, we detected the expression of E-cadherin, N-cadherin,  $\alpha$ -SMA and SNAI1. The results showed that the SNAI1 protein was upregulated to 11.3-fold of the control level, E-cadherin was decreased by 52.8%, and N-cadherin and  $\alpha$ -SMA were increased by a 1.85-fold and 3.07-fold, respectively (Supplementary Fig. 5A), which is in agreement with EEC-EMT. Then we



transfected SNAI1 small interference sequences (si-SNAI1) into  $\Delta$ Np63 $\alpha$  highly expressed EECs for 48 h. The results showed that siRNAs interference with SNAI1 reversed EEC-EMT (Supplementary Fig. 5B). These results further confirm that SNAI1 mediates the EEC-EMT induced by  $\Delta$ Np63 $\alpha$ .

**$\Delta$ Np63 $\alpha$  induces the downregulation of GSK-3 $\beta$  (SNAI1 inhibitor) in EECs and in endometria of IUA patients**

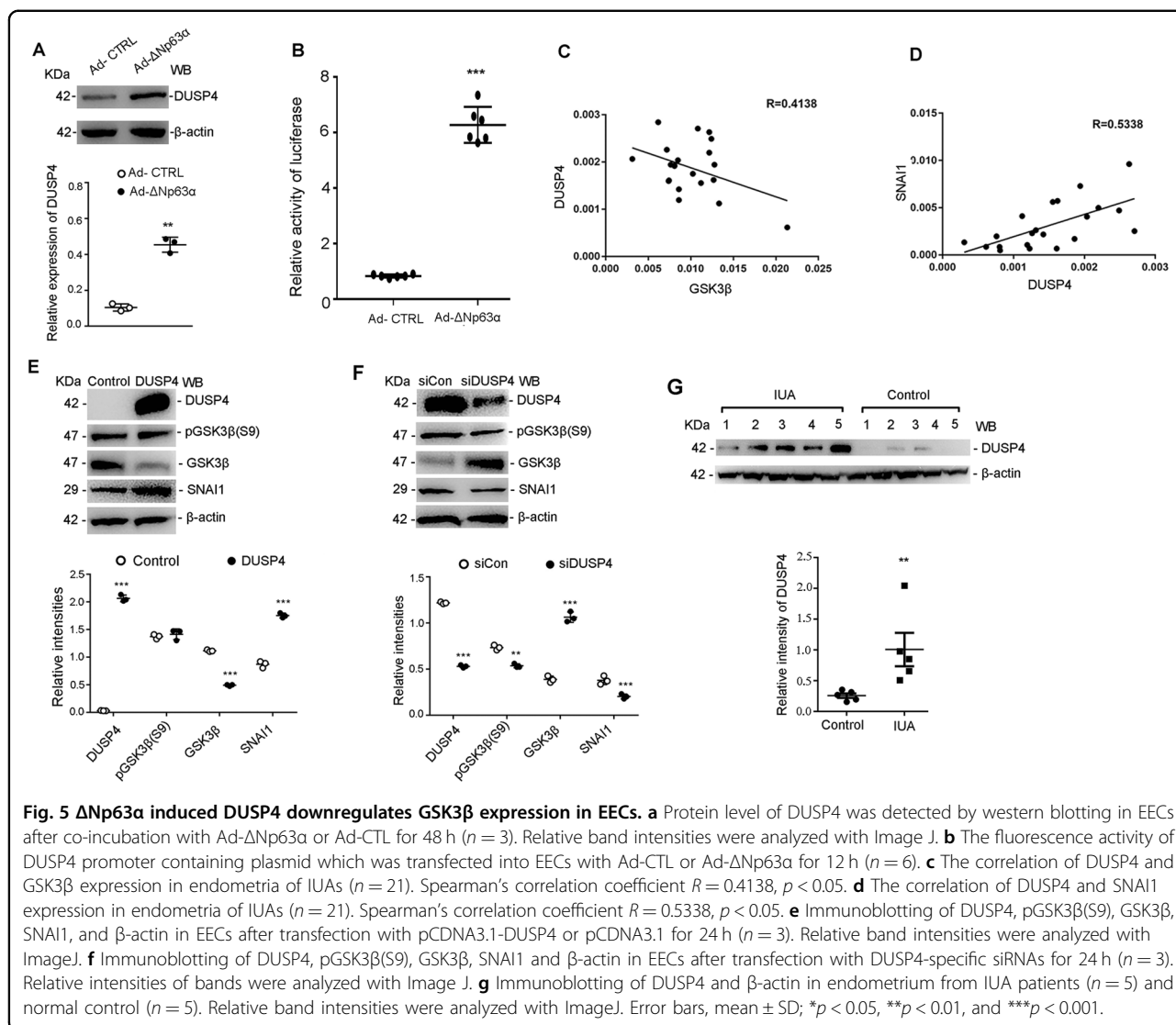
The GSK3 $\beta$ -mediated degradation of SNAI1 is a crucial molecular mechanism that antagonizes EMT<sup>24</sup>. The inhibition of GSK-3 $\beta$  results in the upregulation of SNAI1 and the downregulation of E-cadherin, thus promoting EMT<sup>25</sup>. Since GSK-3 $\beta$  mRNA was downregulated in EECs infected with Ad- $\Delta$ Np63 $\alpha$  (Fig. 2e), we further examined the GSK-3 $\beta$  protein level in Ad- $\Delta$ Np63 $\alpha$ -infected EECs. Western blotting revealed that GSK-3 $\beta$  protein decreased to 49% of that in the cells infected with Ad-CTRL and phospho-GSK3 $\beta$  Ser9 was upregulated by 1.2-fold (Fig. 4a), which is in accordance with the upregulation of SNAI1 protein (Fig. 3a). By treating Ad- $\Delta$ Np63 $\alpha$ -infected EEC with TDZD8 and TWS119 (GSK-3 $\beta$  inhibitors), SNAI1 protein levels in Ad- $\Delta$ Np63 $\alpha$ -infected EEC were 1.8-fold and 2.1-fold higher than those in

Ad-CTRL-infected cells in the presence of TDZD8 and TWS119 (Fig. 4b). Importantly, as showed in Fig. 4c, d, we found the decreased level of GSK-3 $\beta$  and the increased level of inactive form of GSK-3 $\beta$ , p-GSK-3 $\beta$  Ser9, in the endometria from IUA patients, which is consistent with the results obtained in the cultured cells (Fig. 4a).

**$\Delta$ Np63 $\alpha$  induces DUSP4 downregulated GSK3 $\beta$  expression in EECs**

Serine 9 of GSK3 $\beta$  can be phosphorylated by AKT and other kinases<sup>26</sup>, leading to GSK-3 $\beta$  inactivation. Thus, we examined the active form of AKT, pAKT Ser473, in Ad-p63 $\alpha$ -infected EECs and in the endometria from IUA patients. As shown in Supplementary Fig. 6A, the expression of AKT and pAKT Ser473 did not significant change in Ad-p63 $\alpha$ -infected EECs, and both proteins decreased in the endometria of IUA patients (Supplementary Fig. 6B). These results suggested that an alternative pathway existed for  $\Delta$ Np63 $\alpha$ -induced GSK-3 $\beta$  downregulation.

Then we looked back  $\Delta$ Np63 $\alpha$ -induced EEC-transcriptomes, and found that DUSP4 was one of the most upregulated gene, and it was known to be an important EMT promoting molecule<sup>27,28</sup>. To verify the promoting



effect of  $\Delta$ Np63 $\alpha$  on the expression of DUSP4, we measured the protein level of DUSP4 in EECs infected with Ad- $\Delta$ Np63 $\alpha$ , and found that DUSP4 protein was elevated by 1.5-fold (Fig. 5a). To investigate the role of  $\Delta$ Np63 $\alpha$  in promoting DUSP4 expression, we transfected Ad- $\Delta$ Np63 $\alpha$ - or Ad-CTRL-infected EECs with a fluorescence reporter plasmid containing DUSP4 promoter, and compared the fluorescence activity. The results are presented in Fig. 5b, in which fluorescent activity in EECs containing DUSP4 promoter was increased, indicating that  $\Delta$ Np63 $\alpha$  mainly promotes the expression of DUSP4 by acting on its promoter. We further analyzed the correlation between the expression of DUSP4 and GSK3 $\beta$  or SNAI1 respectively in endometria of IUA. The results showed that DUSP4 was negatively correlated with GSK3 $\beta$  ( $R = -0.4138$ ) and positively correlated with SNAI1 ( $R = 0.5338$ ) (Fig. 5c, d).

In order to further investigate the effect of DUSP4 on GSK3 $\beta$ , a DUSP4 expression plasmid (pCDNA3.1-DUSP4) and an empty plasmid (Control) were transfected into primary EECs. Interestingly, overexpressing DUSP4 also downregulated the GSK-3 $\beta$  protein to 32% of the control level. Accordingly, the expression of SNAI1 was 2.7-fold higher than that in the controls (Fig. 5e). However, DUSP4 had no effect on the expression of pGSK3 $\beta$  Ser9 (Fig. 5e). In contrast, by using short siRNAs to interfere with DUSP4 expression in  $\Delta$ Np63 $\alpha$ -overexpressing EECs, the results showed that the downregulation of the DUSP4 protein to 43% of the control level led to a 2.71-fold increase in the total GSK3 $\beta$  protein and a 47.4% and 27.4% decrease in SNAI1 and p-GSK-3 $\beta$  Ser9, respectively (Fig. 5f). Furthermore, we confirmed that DUSP4 protein was significantly increased in the endometrium from IUA

patients compared with that from normal controls (Fig. 5g).

#### **bFGF reverses $\Delta$ Np63 $\alpha$ induced EEC–EMT in vitro**

The data in our present study showed that the pathogenesis of IUA involves EEC–EMT. Previously, we found the proliferation of endometrium is suppressed in  $\Delta$ Np63 $\alpha$  overexpressed endometrium<sup>8</sup>, and bFGF promotes the proliferation of endometrium and functionally reconstructs endometrium in rats and patients<sup>29,30</sup>. Therefore, we tried to study the relationship between bFGF and  $\Delta$ Np63 $\alpha$ -induced EEC–EMT. In the presence of bFGF (0–20 ng/ml),  $\Delta$ Np63 $\alpha$ -infected EECs showed dose-dependent growth, with 10 ng/ml as an optimal concentration (Supplementary Fig. 7A). The expression of  $\Delta$ Np63 $\alpha$ , E-cadherin, N-cadherin,  $\alpha$ -SMA, DUSP4, SNAI1, and GSK3 $\beta$  was detected in  $\Delta$ Np63 $\alpha$ -infected EECs in the presence of bFGF. The results showed that  $\Delta$ Np63 $\alpha$  expression was inhibited by bFGF and the  $\Delta$ Np63 $\alpha$ -induced downregulation of E-cadherin and upregulation of N-cadherin and  $\alpha$ -SMA were reversed by bFGF (Fig. 6a). Furthermore, the  $\Delta$ Np63 $\alpha$ -induced upregulation of DUSP4 and SNAI1 and downregulation of GSK3 $\beta$  were also reversed by bFGF treatment in EECs (Fig. 6b). Further tests with cytometry showed that the cell cycle switched from G0/G1 to S/G2 phase in the presence of bFGF (Fig. 6c, d), with the transcriptional upregulation of CCND1, Ki67, ER $\alpha$  and IGF1 (Fig. 6e) and a slight downregulation of cell apoptosis (Supplementary Fig. 7B), indicating that bFGF reversed Ad- $\Delta$ Np63 $\alpha$ -induced repression of endometrial proliferation and differentiation.

#### **bFGF functionally regenerates endometrium in mice with IUA-like endometrial lesions**

Trauma and inflammation are key factors leading to IUA. In order to generate an IUA mouse model, we injured endometria by mechanical injury and administration of lipopolysaccharide (LPS) in uterine cavity as previously reported<sup>17</sup>. Compared to the sham mice, the mouse model showed the reduction of endometrial glands (Fig. 7a), the accumulation of collagen protein with positive Masson staining (Fig. 7b), the increment of  $\Delta$ Np63 $\alpha$  protein (Fig. 7c), SNAI1 (Fig. 7d), and DUSP4 (Fig. 7e), and the reduction of E-cadherin (Fig. 7f), GSK3 $\beta$  (Fig. 7g), bFGF (Fig. 7h), Ki67 (Fig. 7i), and ER $\alpha$  (Fig. 7j) in the endometria of these mice. These results indicated that the mouse model simulated the endometrial lesions in IUA patients.

Compared to the mouse model treated with PBS, the mice treated with bFGF had functionally regenerated endometrium, with increased endometrial glands (Fig. 7a), alleviated collagen deposition (Fig. 7b), decrement of  $\Delta$ Np63 $\alpha$  protein (Fig. 7c), SNAI1 (Fig. 7d), and DUSP4 (Fig. 7e), and increment of E-cadherin (Fig. 7f), GSK3 $\beta$

(Fig. 7g), bFGF (Fig. 7h), Ki67 (Fig. 7i), and ER $\alpha$  (Fig. 7j) in the endometria of the bFGF-treated mice. The changes in the mRNA levels of these molecules were similar to proteins changes as shown in Supplementary Fig. 8. These results indicated that bFGF reverted the phenotype of IUA-like mouse model.

#### **Discussion**

IUA is characterized with endometrial fibrosis, yet the pathological process is mostly unknown. Here, we demonstrated that EEC–EMT is actively involved in the pathogenesis of endometrial fibrosis. We found for the first time that  $\Delta$ Np63 $\alpha$  drives EEC–EMT by promoting the activity of the SNAI1 pathway and that bFGF reverses  $\Delta$ Np63 $\alpha$ -induced EEC–EMT. The results in the present study provide the potential therapeutic target for IUA patients.

$\Delta$ Np63 $\alpha$  is the predominantly expressed protein isoform of p63 in epithelial cells, which is well-known for its function in maintaining squamous epithelial cell integrity and as an epithelial progenitor cell marker,  $\Delta$ Np63 $\alpha$  regulated keratinocytes regeneration<sup>31,32</sup>. Previous studies showed the expression of p63 turns off in endometrium after the fusion of bilateral paramesonephric ducts<sup>10</sup>. In the present study, we found that EECs ectopically expressed  $\Delta$ Np63 $\alpha$  in patients with IUA, which was further confirmed by the co-localization staining of  $\Delta$ Np63 $\alpha$  with CK and E-cadherin in EECs. Several studies indicated that p63 expression is related to tissue fibrosis, in which EMT plays a critical role. In early stage of idiopathic pulmonary fibrosis, increased expression of  $\Delta$ Np63 $\alpha$  in bronchopulmonary epithelium can promote EMT, resulting in lung fibrosis<sup>33</sup>. High expression of  $\Delta$ Np63 $\alpha$  in sublingual gland epithelial cells can also lead to EMT and promote fibrosis<sup>34–37</sup>.

In the present study, we found that the expression of  $\Delta$ Np63 $\alpha$  in EECs causes type 2 EMT. This is supported by the hybrid phenotype with both epithelial and mesenchymal traits in upregulated  $\Delta$ Np63 $\alpha$  EECs in severe IUA patients, which was validated by the downregulation of E-cadherin (epithelial marker) and the upregulation of N-cadherin, Vimentin, and  $\alpha$ -SMA (mesenchymal markers) in  $\Delta$ Np63 $\alpha$  overexpressed EECs and IUA-like mouse model.

In searching how  $\Delta$ Np63 $\alpha$  expression in EECs causes type 2 EMT, we found that  $\Delta$ Np63 $\alpha$  upregulates the transcription factor SNAI1, and downregulates GSK-3 $\beta$ . SNAI1 is an important inducer of EMT<sup>38</sup>. GSK-3 $\beta$  is an inhibitory kinase of SNAI1 and increment of GSK-3 $\beta$  in the cells can block EMT process by enhancing degrading SNAI1<sup>25</sup>. In addition, we also found that upregulation of  $\Delta$ Np63 $\alpha$  increases DUSP4, and the DUSP4 expression is negatively correlated with the GSK-3 $\beta$  level in EECs. The overexpression of DUSP4 in EECs mimicked  $\Delta$ Np63 $\alpha$ -

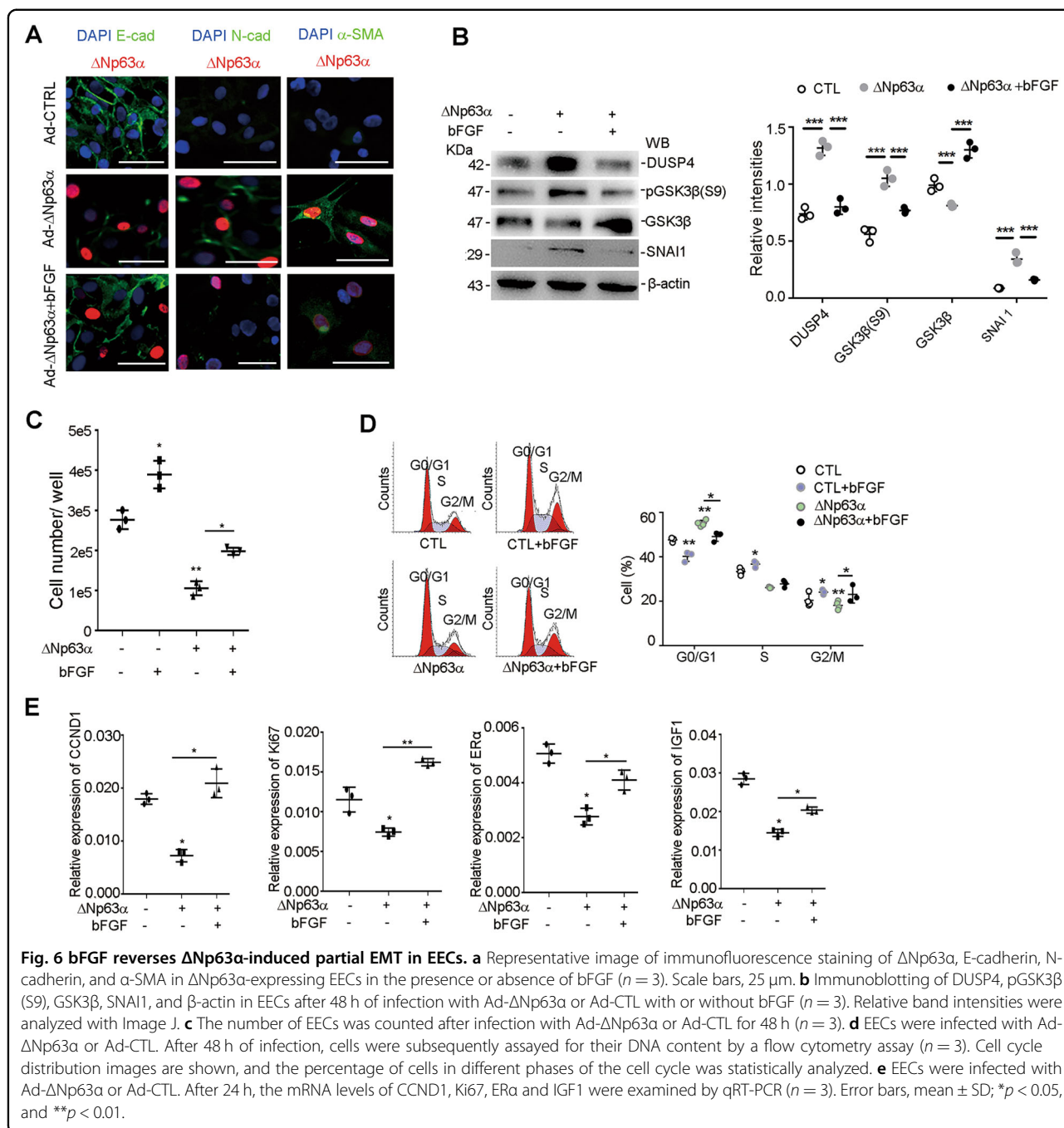


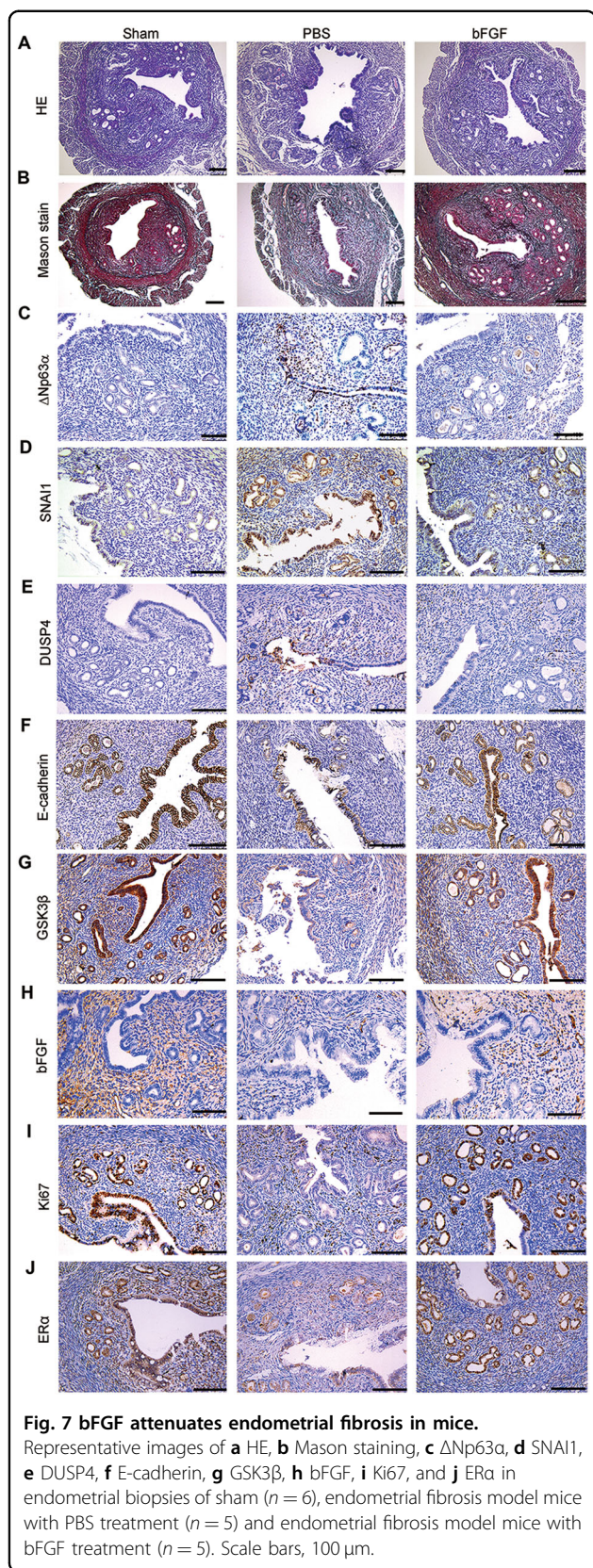
**Fig. 6** bFGF reverses  $\Delta$ Np63 $\alpha$ -induced partial EMT in EECs. **a** Representative image of immunofluorescence staining of  $\Delta$ Np63 $\alpha$ , E-cadherin, N-cadherin, and  $\alpha$ -SMA in  $\Delta$ Np63 $\alpha$ -expressing EECs in the presence or absence of bFGF ( $n = 3$ ). Scale bars, 25  $\mu$ m. **b** Immunoblotting of DUSP4, pGSK3 $\beta$  (S9), GSK3 $\beta$ , SNAI1, and  $\beta$ -actin in EECs after 48 h of infection with Ad- $\Delta$ Np63 $\alpha$  or Ad-CTRL with or without bFGF ( $n = 3$ ). Relative band intensities were analyzed with Image J. **c** The number of EECs was counted after infection with Ad- $\Delta$ Np63 $\alpha$  or Ad-CTRL for 48 h ( $n = 3$ ). **d** EECs were infected with Ad- $\Delta$ Np63 $\alpha$  or Ad-CTRL. After 48 h of infection, cells were subsequently assayed for their DNA content by a flow cytometry assay ( $n = 3$ ). Cell cycle distribution images are shown, and the percentage of cells in different phases of the cell cycle was statistically analyzed. **e** EECs were infected with Ad- $\Delta$ Np63 $\alpha$  or Ad-CTRL. After 24 h, the mRNA levels of CCND1, Ki67, ER $\alpha$  and IGF1 were examined by qRT-PCR ( $n = 3$ ). Error bars, mean  $\pm$  SD; \* $p < 0.05$ , and \*\* $p < 0.01$ .

induced EEC-EMT, and inhibition of DUSP4 reversed EEC-EMT, indicating the important role of DUSP4 in EEC-EMT. Nevertheless, the detailed molecular process requires further studies.

Of the 69 patients initially enrolled, 43.5% (30/69) had detectable mRNA and protein of  $\Delta$ Np63, 30.4% (21/69) had no detectable mRNA and protein, and some patients just showed detectable mRNA or protein. There are several possibilities for the disagreement in the detection of mRNA and protein in these patients. The undetectability

of mRNA and protein in 21 patients may reflect that there is no expression of  $\Delta$ Np63 $\alpha$ , the expression level is too low to be detected, or the expression is focalized so that the sampling missed the foci that express  $\Delta$ Np63 $\alpha$ . Probably, because of the focalized expression of  $\Delta$ Np63 $\alpha$ , the results of mRNA and IHC were not in agreement in some patients.

bFGF functions to enhance the tissue repair. Recently, in vitro study showed that bFGF inhibits the transition of fibroblast to myofibroblast<sup>39</sup>. In the human, we previously



demonstrated that bFGF has the activity against fibrosis in fibrotic endometria<sup>29</sup>. In the present study, the administration of bFGF in IUA-like mice improved the endometrial fibrosis while  $\Delta$ Np63 $\alpha$  and SNAI1 levels in EECs were reduced, and E-cadherin was increased and N-cadherin and  $\alpha$ -SMA were decreased. These results provided solid evidence that  $\Delta$ Np63 $\alpha$  plays an important role in the pathogenesis of IUA and that  $\Delta$ Np63 $\alpha$  may serve as a potential target for IUA therapy.

**Acknowledgements**

This study was supported by research grants from The Strategic Priority Research Program of the Chinese Academy of Sciences (XDA16040300), Excellent Youth Natural Science Foundation of Jiangsu Province (BK20170051), National Natural Science Foundation of China (81771526 and 81971336), Jiangsu Province's Key Provincial Talents Program (ZDRCA2016067), Jiangsu Provincial Key Medical Center (YXZXB2016004), and National Key R&D Program of China (2018YFC1004404).

**Author details**

<sup>1</sup>Department of Obstetrics and Gynecology, The Affiliated Drum Tower Hospital of Nanjing University Medical School, 321 Zhongshan Rd., Nanjing 210008, China. <sup>2</sup>Department of Laboratory Medicine, Jiangsu Key Laboratory for Molecular Medicine, Nanjing University Medical School, 321 Zhongshan Rd., Nanjing 210008, China. <sup>3</sup>Department of Obstetrics and Gynecology, Nanjing Drum Tower Hospital, Peking Union Medical College, Chinese Academy of Medical Science, Graduate School of Peking Union Medical College, Nanjing 210008, China. <sup>4</sup>Department of Obstetrics and Gynecology, Drum Tower Clinical Medical College, Nanjing Medical University, Nanjing 210000, China. <sup>5</sup>Institute of Genetics and Developmental Biology, Chinese Academy of Sciences, 3 Nanyitiao, Zhongguancun, Beijing 100190, China. <sup>6</sup>Department of Obstetrics, Gynecology and Reproductive Sciences, Center for Reproductive Sciences, Eli and Edythe Broad Center of Regeneration Medicine and Stem Cell Research, University of California San Francisco, San Francisco, CA 94131, USA

**Conflict of interest**

The authors declare that they have no conflict of interest.

**Publisher's note**

Springer Nature remains neutral with regard to jurisdictional claims in published maps and institutional affiliations.

**Supplementary Information** accompanies this paper at (<https://doi.org/10.1038/s41419-020-2666-y>).

Received: 26 February 2020 Revised: 29 May 2020 Accepted: 3 June 2020  
Published online: 11 June 2020

**References**

1. Macara, I. G., Guyer, R., Richardson, G., Huo, Y. & Ahmed, S. M. Epithelial homeostasis. *Curr. Biol.* **24**, 11 (2014).
2. Tai, K., Cockburn, K. & Greco, V. Flexibility sustains epithelial tissue homeostasis. *Curr. Opin. Cell Biol.* **60**, 8 (2019).
3. Takahashi, N. et al. RIPK1 ensures intestinal homeostasis by protecting the epithelium against apoptosis. *Nature* **513**, 5 (2014).
4. Evans, J. et al. Fertile ground: human endometrial programming and lessons in health and disease. *Nat. Rev. Endocrinol.* **12**, 654–667 (2016).
5. Yu, D., Wong, Y. M., Cheong, Y., Xia, E. & Li, T. C. Asherman syndrome-one century later. *Fertil. Steril.* **89**, 759–779 (2008).
6. Santamaria, X., Isaacson, K. & Simón, C. Asherman's syndrome: it may not be all our fault. *Hum. Reprod.* **33**, 1374–1380 (2018).
7. Nieto, M. A., Huang, R. Y., Jackson, R. A. & Thiery, J. P. EMT: 2016. *Cell* **166**, 21–45 (2016).

8. Zhao, G. et al. Transplantation of collagen scaffold with autologous bone marrow mononuclear cells promotes functional endometrium reconstruction via downregulating DeltaNp63 expression in Asherman's syndrome. *Sci. China Life Sci.* **60**, 404–416 (2017).
9. Vanbokhoven, H., Melino, G., Candi, E. & Declercq, W. p63, a Story of Mice and Men. *J. Invest. Dermatol.* **131**, 1196–1207 (2011).
10. Aplin, J. D., Asgerally, T. F. & Fazleabas, A. T. *The Endometrium: Molecular, Cellular and Clinical Perspectives Second Edition*. (Informa Healthcare Press, UK, 2008).
11. Zuo, W. et al. p63(+)/Krt5(+) distal airway stem cells are essential for lung regeneration. *Nature* **517**, 616–620 (2015).
12. Vaughan, A. E. et al. Lineage-negative progenitors mobilize to regenerate lung epithelium after major injury. *Nature* **517**, 621–625 (2015).
13. The American Fertility Society. The American Fertility Society Classifications of Adnexal Adhesions, distal tubal occlusion, secondary to tubal ligation, tubal pregnancies, mullerian anomalies and intrauterine adhesions. *Fertil. Steril.* **49**, 12 (1988).
14. Perteu, M., Kim, D., Perteu, G. M., Leek, J. T. & Salzberg, S. L. Transcript-level expression analysis of RNA-seq experiments with HISAT, StringTie and Ballgown. *Nat. Protoc.* **11**, 18 (2016).
15. Kim, D., Langmead, B. & Salzberg, S. L. HISAT: a fast spliced aligner with low memory requirements. *Nat. Methods* **12**, 4 (2015).
16. Trapnell, C. et al. Differential gene and transcript expression analysis of RNA-seq experiments with TopHat and Cufflinks. *Nat. Protoc.* **7**, 7 (2012).
17. Li, J. et al. MicroRNA-29b inhibits endometrial fibrosis by regulating the Sp1-TGF- $\beta$ 1/Smad-CTGF axis in a rat. *Model. Reprod. Sci.* **23**, 9 (2016).
18. Walmer, D. K., Wrona, M. A., Hughes, C. L. & Nelson, K. G. Lactoferrin expression in the mouse reproductive tract during the natural estrous cycle: correlation with circulating estradiol and progesterone. *Endocrinology* **131**, 9 (1992).
19. Wood, G. A., Fata, J. E., Watson, K. L. & Khokha, R. Circulating hormones and estrous stage predict cellular and stromal remodeling in murine uterus. *Reproduction* **133**, 10 (2007).
20. Cebrià-Costa, J. P., Millanes-Romero, A., de Herreros, A. G. & Peiró S. The epithelial-to-mesenchymal transition (EMT), a particular case. *Mol. Cell Oncol.* **1** (2014).
21. Vitalone, M. J. et al. The dual role of epithelial-to-mesenchymal transition in chronic allograft injury in pediatric renal transplantation. *Transplantation* **92**, 787–795 (2011).
22. Dominguez, C., David, J. M. & Palena, C. Epithelial-mesenchymal transition and inflammation at the site of the primary tumor. *Semin. Cancer Biol.* **47**, 8 (2017).
23. Baek, S. T. & Tallquist, M. D. Nf1 limits epicardial derivative expansion by regulating epithelial to mesenchymal transition and proliferation. *Development* **139**, 10 (2012).
24. Liu, Y. et al. SPSB3 targets SNAIL for degradation in GSK-3 $\beta$  phosphorylation-dependent manner and regulates metastasis. *Oncogene* **37**, 9 (2018).
25. Zhou, B. P. et al. Dual regulation of Snail by GSK-3 $\beta$ -mediated phosphorylation in control of epithelial-mesenchymal transition. *Nat. Cell Biol.* **6**, 10 (2004).
26. Beurel, E., Grieco, S. F. & Jope, R. S. Glycogen synthase kinase-3 (GSK3): regulation, actions, and diseases. *Pharm. Ther.* **148**, 18 (2015).
27. Liu, Y. et al. Knockdown of dual specificity phosphatase 4 enhances the chemosensitivity of MCF-7 and MCF-7/ADR breast cancer cells to doxorubicin. *Cell Res.* **319**, 3140–3149 (2013).
28. Du, F. et al. miR-137 alleviates doxorubicin resistance in breast cancer through inhibition of epithelial-mesenchymal transition by targeting DUSP4. *Cell Death Dis.* **10**, 922 (2019).
29. Jiang, P., et al. Collagen-binding basic fibroblast growth factor improves functional remodeling of scarred endometrium in uterine infertile women: a pilot study. *Sci China Life Sci.* **62**, 1617–1629 (2019).
30. Li, X. et al. Regeneration of uterine horns in rats by collagen scaffolds loaded with collagen-binding human basic fibroblast growth factor. *Biomaterials* **10**, 32 (2011).
31. Koster, M. I., Kim, S., Mills, A. A., DeMayo, F. J. & Roop, D. R. p63 is the molecular switch for initiation of an epithelial stratification program. *Genes Dev.* **18**, 126–131 (2004).
32. Koster, M. I., et al. p63 induces key target genes required for epidermal morphogenesis. *Proc. Natl Acad. Sci. USA* **104**, 3255–3260 (2007).
33. Murata, K., et al. p63—key molecule in the early phase of epithelial abnormality in idiopathic pulmonary fibrosis. *Exp. Mol. Pathol.* **83**, 367–376 (2007).
34. Haniffa, A. M. et al. Expression pattern of p63 in oral epithelial lesions and submucous fibrosis associated with betel-quid chewing in sri lanka. *Med Mol. Morphol.* **40**, 203–207 (2007).
35. Varun, B. R., Ranganathan, K., Rao, U. K. & Joshua, E. Immunohistochemical detection of p53 and p63 in oral squamous cell carcinoma, oral leukoplakia, and oral submucous fibrosis. *J. Investig. Clin. Dent.* **5**, 214–219 (2014).
36. Das, R. K. et al. Assessment of malignant potential of oral submucous fibrosis through evaluation of p63, E-cadherin and CD105 expression. *J. Clin. Pathol.* **63**, 894–899 (2010).
37. Das, R. K. et al. Epithelio-mesenchymal transitional attributes in oral submucous fibrosis. *Exp. Mol. Pathol.* **95**, 259–269 (2013).
38. Tian, B. et al. BRD4 mediates NF- $\kappa$ B-dependent epithelial-mesenchymal transition and pulmonary fibrosis via transcriptional elongation. *Am. J. Physiol. Lung Cell Mol. Physiol.* **311**, 19 (2016).
39. Dolivo, D. M., Larson, S. A. & Dominko, T. FGF2-mediated attenuation of myofibroblast activation is modulated by distinct MAPK signaling pathways in human dermal fibroblasts. *J. Dermatol. Sci.* **88**, 339–348 (2017).